

# Semantically Self-Aligned Network for Text-to-Image Part-aware Person Re-identification

Zefeng Ding<sup>1</sup> Changxing Ding<sup>1,2\*</sup> Zhiyin Shao<sup>1</sup> Dacheng Tao<sup>3</sup>

<sup>1</sup> South China University of Technology <sup>2</sup> Pazhou Lab, Guangzhou <sup>3</sup> JD Explore Academy

{eezefengding@mail., chxding@, eezyshao@mail.}@scut.edu.cn, dacheng.tao@jd.com

## Abstract

*Text-to-image person re-identification (ReID) aims to search for images containing a person of interest using textual descriptions. However, due to the significant modality gap and the large intra-class variance in textual descriptions, text-to-image ReID remains a challenging problem. Accordingly, in this paper, we propose a Semantically Self-Aligned Network (SSAN) to handle the above problems. First, we propose a novel method that automatically extracts semantically aligned part-level features from the two modalities. Second, we design a multi-view non-local network that captures the relationships between body parts, thereby establishing better correspondences between body parts and noun phrases. Third, we introduce a Compound Ranking (CR) loss that makes use of textual descriptions for other images of the same identity to provide extra supervision, thereby effectively reducing the intra-class variance in textual features. Finally, to expedite future research in text-to-image ReID, we build a new database named ICFG-PEDES. Extensive experiments demonstrate that SSAN outperforms state-of-the-art approaches by significant margins. Both the new ICFG-PEDES database and the SSAN code are available at <https://github.com/zifyloo/SSAN>.*

## 1. Introduction

Text-to-image person re-identification (ReID) refers to searching for images containing a person of interest (e.g. a missing child) based on natural language descriptions. It is a vital and valuable video surveillance tool when there are no probe images of the target person and only textual descriptions are available [17]. Unfortunately, the majority of the existing ReID literature focuses on image-based ReID, with text-to-image ReID still in its infancy [34, 15].

Text-to-image ReID is much more challenging than image-based ReID. One of the main reasons for this is that

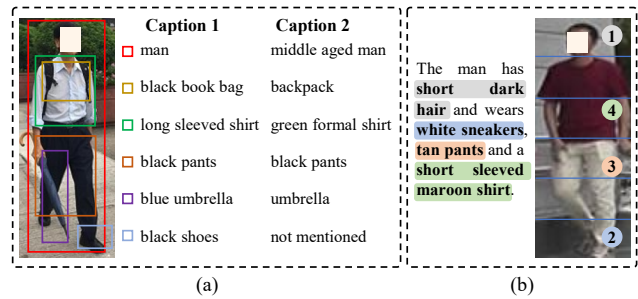


Figure 1. Textual descriptions are free-form, which introduces unique challenges to text-to-image ReID. (a) Textual descriptions for the same image may vary dramatically. (b) Body parts may be described in an arbitrary order. The numbers in this figure indicate the order in which the body parts are described.

textual descriptions are free-form, which creates two main problems. First, as illustrated in Figure 1(a), textual descriptions of the same image may vary dramatically, leading to large intra-class variance in textual features. Second, body parts are usually well aligned after pedestrian detection; however, as illustrated in Figure 1(b), body parts may be described in an arbitrary order, thereby introducing semantic misalignment between visual and textual features.

Accordingly, cross-modal alignment is crucial for text-to-image ReID. One popular cross-modal alignment strategy involves adopting attention models to acquire correspondences between body parts and words [17, 16, 2]. However, this strategy depends on cross-modal operations for each image-text pair, which are computationally expensive [24]. Another intuitive strategy involves splitting one textual description into several groups of noun phrases by using external tools, e.g. the Natural Language Toolkit [20]. Each group of noun phrases corresponds to one specific body part [11, 21, 32]. The downside of this approach is that the quality of textual feature is sensitive to the reliability of the external tools. Furthermore, the splitting operation destroys correlations between noun phrases, degrading the quality of textual feature.

\*Corresponding author.

In this paper, we propose a novel model, named Semantically Self-Aligned Network (SSAN), which efficiently extracts semantically aligned visual and textual features. SSAN does not split the textual description or perform cross-modal operations; instead, it explores the relatively well aligned body parts in images and uses them as supervision to achieve this goal. More specifically, we first process each textual description with a bidirectional long short-term memory network (Bi-LSTM) [9] to capture the relationships among the words. With the aid of contextual cues, we infer the word-part correspondences using a Word Attention Module (WAM) based on the representation of each word. Accordingly, we can obtain the raw part-level textural features with reference to the word-part correspondences. The raw part-level textual features are further refined by a shared  $1 \times 1$  convolutional (Conv) layer between the two modalities. Finally, by constraining the part-level features from both modalities to be similar, WAM is forced to make reasonable predictions and the semantic gap between the two modalities is reduced.

However, the above model ignores correlations between body parts. In textual descriptions, one noun phrase often covers several body parts (e.g. “long dress”). Moreover, textual descriptions may specify certain spatial relationships between image regions (e.g. “holding a bag”). Accordingly, we propose a multi-view non-local network (MV-NLN) based on the non-local attention mechanism [31] to capture the relationships between body parts. Briefly, we first compute the similarity between the  $k$ -th part feature and each of the other part features in a shared embedding space via multi-view projection. Next, the similarity scores specify the strength of the interactions between the  $k$ -th part and the other parts. After interaction, the receptive field of each part feature extends to become more consistent with the noun phrases.

Furthermore, to overcome the intra-class variance in the descriptions, we propose a Compound Ranking (CR) loss. In traditional ranking loss [4], positive pairs are composed of exactly matched image-text pairs. Motivated by the observation that one textual description can roughly annotate other images of the same identity, the CR loss adopts them to compose weakly supervised terms to optimize the network. However, the descriptive power of this rough annotation varies dramatically, depending on both the quality of the text and the difference in appearance between two images. Accordingly, we propose a strategy to adaptively adjust the margin for the new loss terms. The CR loss can be considered as a novel data augmentation method.

Finally, as there is only one large-scale database available (i.e., CUHK-PEDES [17]), we build a new database named Identity-Centric and Fine-Grained Person Description Dataset (ICFG-PEDES) for text-to-image ReID. Compared with CUHK-PEDES, our new database has three

key advantages. First, its textual descriptions are identity-centric and fine-grained; in comparison, the textual descriptions contained in CUHK-PEDES are relatively short and may contain identity-irrelevant details (such as actions and backgrounds). More specifically, ICFG-PEDES has 58% more words per caption on average than CUHK-PEDES. Second, the images included in ICFG-PEDES are more challenging, containing more appearance variability due to the presence of complex backgrounds and variable illumination [35]. Third, the scale of ICFG-PEDES is larger: it contains 36% more images than CUHK-PEDES. In future, we intend to release the ICFG-PEDES database, which is expected to further expedite research in text-to-image ReID.

We conduct extensive experiments on both the ICFG-PEDES and CUHK-PEDES databases. The results show that SSAN outperforms existing approaches by large margins. Moreover, SSAN has further advantages in terms of efficiency and ease of use.

## 2. Related Work

Image-text retrieval is an important vision and language task. To obtain aligned features from the two modalities, early works typically projected holistic images and textual descriptions into a shared feature space [5, 30, 7, 13, 37]. For example, Frome *et al.* [5] proposed to learn linear transformations for image features and skip-gram word features, with a ranking loss employed to aid optimization. More recent approaches have further established accurate correspondences between image regions and words [1, 10, 14, 23, 39, 36, 18, 33]. For example, Zhang *et al.* [39] considered both the interactions between the two modalities and semantic relationships in a single modality. Briefly, they adopted a region-to-word attention model to align cross-modal features, while also utilizing a second-order attention model to explore intra-modal correlations.

Due to its fine-grained nature, text-to-image ReID is one of the most challenging image-text retrieval tasks. Depending on the strategy used to align cross-modal features, existing works can be divided into two categories as follows:

**Novel Model Structures.** These works usually design various attention-based models to establish region-word [17, 16, 2] or region-phrase [11, 21] correspondences. For example, as a region-word-based method, Chen *et al.* [2] proposed a model that computed the affinity between each word and image region pair. They then selected the best matching image region for each word. The final image-text affinity score was obtained via a word attention sub-network. Among the region-phrase-based methods, Niu *et al.* [21] proposed a cross-modal attention model to align features from the two modalities at the global-to-global, global-to-local, and local-to-local levels in order to extract multi-granular features. However, these works require cross-modal operations for each image-text pair, which in-

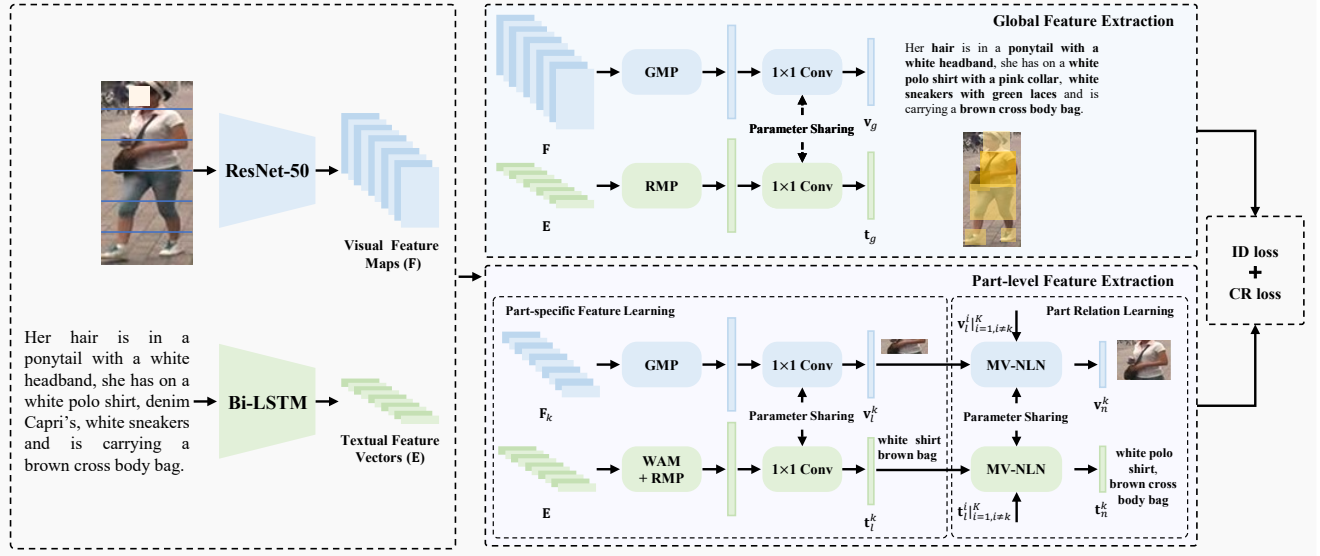


Figure 2. The SSAN model architecture. Based on the ResNet-50 and Bi-LSTM backbones, SSAN extracts global and part features respectively from both modalities. For simplicity, only the global branch and the  $k$ -th part branch are shown.  $k$  is equal to 3 in this figure. The other  $K-1$  part branches have the same structure as the  $k$ -th one. For the global branch, we adopt a weight sharing strategy on the last  $1 \times 1$  Conv layer, which aligns the features from the two modalities more tightly in terms of semantics. Each part branch includes one Part-specific Feature Learning (PFL) module and one Part Relation Learning (PRL) module. The former module enables SSAN to automatically extract part-level features from both modalities, without using any external tools or cross-modal operations; the latter enables SSAN to capture the relationships between body parts so as to establish better semantic correspondences with noun phrases.

roduces a high computational cost [24]. Recently, Wang *et al.* [32] proposed an approach that is free from cross-modal operations. They aligned body parts with noun phrases with the help of an auxiliary segmentation layer and an external toolkit for sentence parsing. However, the textual features' quality relies on the reliability of the external tools.

**New Optimization Strategies.** These works utilize various objective functions to optimize text-to-image ReID models [16, 4, 26, 40, 41, 19, 6]. For example, Faghri *et al.* [4] proposed a ranking loss to minimize the intra-class distance and maximize the inter-class distance. Sarafianos *et al.* [26] adopted an adversarial loss to drive textual features to be close enough to visual features such that a modality discriminator could not distinguish the two. Zheng *et al.* [41] proposed an instance loss that achieved better inter-modal alignment by sharing classifiers for the two modalities. However, these methods do not explicitly solve the significant intra-class variance problem in the textual modality.

### 3. Semantically Self-Aligned Network

The overall architecture of SSAN is illustrated in Figure 2. In what follows, we first introduce the backbone for representation extraction in Section 3.1 and then describe the branches for global and part feature learning in Sections 3.2 and 3.3, respectively.

#### 3.1. Backbone

**Visual Representation Extraction:** We adopt the popular ResNet-50 [8] model as the visual feature extraction backbone. As shown in Figure 2, we first extract the feature maps  $\mathbf{F} \in \mathbb{R}^{H \times W \times C}$ , where  $H$ ,  $W$ , and  $C$  represent the height, width, and channel number of the feature maps, respectively. For the global branch, we directly utilize  $\mathbf{F}$  to learn the global visual feature. For the part branches, we first uniformly partition  $\mathbf{F}$  into  $K$  non-overlapping parts  $\mathbf{F}_k \in \mathbb{R}^{C \times H' \times W}$  ( $1 \leq k \leq K$ ), following [28]. We then extract the part-level visual features from  $\mathbf{F}_k$ .

**Textual Representation Extraction:** We build a matrix  $\mathbf{W}_e \in \mathbb{R}^{V \times U}$  containing word embeddings of all unique words in the training set. Here,  $V$  and  $U$  denote the word embedding dimension and the number of unique words, respectively. Given a description  $\mathbf{D}$  of length  $n$ , we obtain the word embedding  $\mathbf{x}_i \in \mathbb{R}^V$  for its  $i$ -th word from  $\mathbf{W}_e$ .

To capture the relationships among the words, we adopt a bidirectional long short-term memory network (Bi-LSTM) [9] as our textual backbone. Bi-LSTM processes word embeddings from both  $\mathbf{x}_1$  to  $\mathbf{x}_n$  and  $\mathbf{x}_n$  to  $\mathbf{x}_1$  as follows:

$$\vec{\mathbf{h}}_i = \overrightarrow{LSTM}(\mathbf{x}_i, \vec{\mathbf{h}}_{i-1}), \quad (1)$$

$$\overleftarrow{\mathbf{h}}_i = \overleftarrow{LSTM}(\mathbf{x}_i, \overleftarrow{\mathbf{h}}_{i+1}), \quad (2)$$

where  $\vec{\mathbf{h}}_i, \overleftarrow{\mathbf{h}}_i \in \mathbb{R}^C$  and represent the forward and backward hidden states of the  $i$ -th word, respectively. Next, the

representation for the  $i$ -th word is defined as follows:

$$\mathbf{e}_i = \frac{\vec{\mathbf{h}}_i + \overleftarrow{\mathbf{h}}_i}{2}. \quad (3)$$

Finally, we stack  $\mathbf{e}_i (1 \leq i \leq n)$  to represent the textual description  $\mathbf{D}$ , as follows:

$$\mathbf{E} = [\mathbf{e}_1, \mathbf{e}_2, \dots, \mathbf{e}_n], \quad (4)$$

where  $\mathbf{E} \in \mathbb{R}^{C \times n}$ .

### 3.2. Global Feature Extraction

Following the recent works [11, 21, 32], SSAN also projects holistic visual and textual features into a common space. To obtain the global features, we first perform Global Max Pooling (GMP) on  $\mathbf{F}$  and Row-wise Max Pooling (RMP) on  $\mathbf{E}$ . We then project the obtained features into a common feature space via a shared  $1 \times 1$  Conv layer  $\mathbf{W}_g$ :

$$\mathbf{v}_g = \mathbf{W}_g \text{GMP}(\mathbf{F}), \quad (5)$$

$$\mathbf{t}_g = \mathbf{W}_g \text{RMP}(\mathbf{E}), \quad (6)$$

where  $\mathbf{W}_g \in \mathbb{R}^{M \times C}$ .  $\mathbf{v}_g, \mathbf{t}_g \in \mathbb{R}^M$  and represent the global visual and textual features. Compared to previous methods [11, 32], the weight-sharing strategy on  $\mathbf{W}_g$  encourages  $\mathbf{F}$  and  $\mathbf{E}$  to be more tightly aligned in terms of semantics. In this way, our global branch outperforms that presented in [11, 32], as demonstrated in experiment below.

Eventually, the similarity between global features of one image-text pair is denoted as follows:

$$S_g = \frac{\mathbf{v}_g^T \mathbf{t}_g}{\|\mathbf{v}_g\| \|\mathbf{t}_g\|}. \quad (7)$$

### 3.3. Part-level Feature Extraction

Part-level representations are essential for ReID [11, 21, 32]. However, as explained in Figure 1, extracting part-level textual features is challenging. Therefore, we introduce the part branches in SSAN that efficiently extract semantically aligned part-level visual and textual features. Each part branch includes one Part-specific Feature Learning (PFL) module and one Part Relation Learning (PRL) module.

#### 3.3.1 Part-specific Feature Learning

To obtain part-level textual features, existing approaches [11, 21, 32] usually first detect noun phrases using external tools and then extract textual features for each part. However, this strategy breaks textual context. For example, as illustrated in Figure 3(a), the noun phrase “white line” may relate to different items of clothing or accessories; without textual context, the correspondence between “white line” and body parts cannot be inferred.

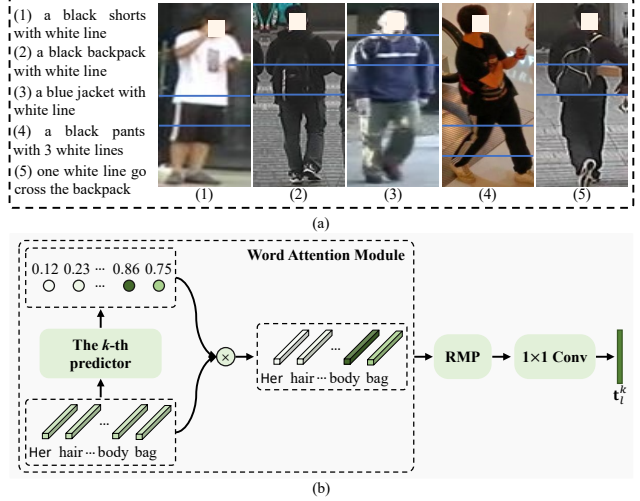


Figure 3. (a) The same noun phrase (e.g., “white line”) can be associated with different items of clothing or accessories. (b) The WAM model structure. We take the  $k$ -th part branch as an example. In this figure,  $k$  is equal to 3.

It is therefore highly desirable to extract part-level textual features directly from the original textual description without external tools. As shown in Figure 3(a), the body parts in images are usually well-aligned. Therefore, we utilize the well-aligned human body parts as supervision to facilitate achieving this goal. Furthermore, we argue that after the LSTM processing is complete,  $\mathbf{e}_i$  will have obtained contextual cues that can be used to infer which part the  $i$ -th word corresponds to. Accordingly, we propose the following approach for the efficient extraction of semantically aligned part-level visual and textual features.

First, we introduce the Word Attention Module (WAM) to infer the word-part correspondences. As illustrated in Figure 3(b), we predict the probability that the  $i$ -th word belongs to the  $k$ -th part as follows:

$$s_i^k = \sigma(\mathbf{W}_p^k \mathbf{e}_i), \quad (8)$$

where  $s_i^k$  denotes the probability and  $\sigma$  stands for the sigmoid function.  $\mathbf{W}_p^k \in \mathbb{R}^{1 \times C}$ . We modify  $\mathbf{E}$  to represent the textual description for the  $k$ -th part as follows:

$$\mathbf{E}_k = [s_1^k \mathbf{e}_1, s_2^k \mathbf{e}_2, \dots, s_n^k \mathbf{e}_n]. \quad (9)$$

Second, as illustrated in Figure 2, we obtain the visual features for the  $k$ -th part by feeding  $\mathbf{F}_k$  into one GMP layer and one  $1 \times 1$  Conv layer. Similarly, we generate the  $k$ -th part-level textual features by performing RMP on  $\mathbf{E}_k$  and feed it to the same  $1 \times 1$  Conv layer as  $\mathbf{F}_k$ . Formally,

$$\mathbf{v}_i^k = \mathbf{W}_i^k \text{GMP}(\mathbf{F}_k), \quad (10)$$

$$\mathbf{t}_i^k = \mathbf{W}_i^k \text{RMP}(\mathbf{E}_k), \quad (11)$$

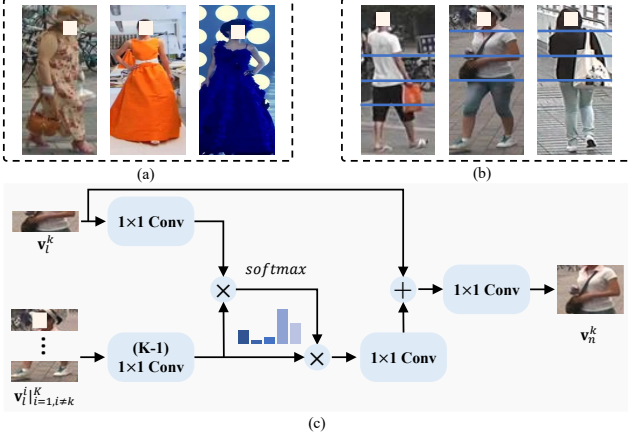


Figure 4. (a) One noun phrase may cover two or more equally divided body parts, e.g. “long dress”. (b) Textural descriptions may include relationships between parts or image regions, e.g. “holding a bag”. (c) The MV-NLN model structure. We take the  $k$ -th visual part feature  $\mathbf{v}_l^k$  as an example. In this figure,  $k$  is equal to 4.

where  $\mathbf{W}_l^k \in \mathbb{R}^{M \times C}$  and denotes the parameters of the shared  $1 \times 1$  Conv layer.  $\mathbf{v}_l^k, \mathbf{t}_l^k \in \mathbb{R}^M$  and represent the visual and textual features for the  $k$ -th part, respectively.

By constraining  $\mathbf{v}_l^k$  and  $\mathbf{t}_l^k$  to be both discriminative and similar, WAM is forced to make reasonable predictions about word-part correspondences. It is worth noting that one word may correspond to several parts, as explained in Figure 4(a). Moreover, the shared  $1 \times 1$  Conv layer is forced to select elements relevant to the  $k$ -th part from  $\mathbf{F}_k$  and  $\mathbf{E}_k$ . In this way, we can obtain semantically aligned part-level visual and textual features without any external tools.

Finally, the similarity between the part-level features of one image-text pair is denoted as follows:

$$S_l = \frac{\mathbf{v}_l^T \mathbf{t}_l}{\|\mathbf{v}_l\| \|\mathbf{t}_l\|}, \quad (12)$$

where  $\mathbf{v}_l$  and  $\mathbf{t}_l \in \mathbb{R}^{KM}$ . They are obtained by concatenating the  $K$  part-level visual and textual features, respectively.

### 3.3.2 Part Relation Learning

The equal partition strategy on  $\mathbf{F}$  is effective for image-based ReID [28, 38, 3, 29]. However, it maybe suboptimal for text-to-image ReID, as one phrase may cover two or more equally divided parts (e.g. “long dress” in Figure 4(a)). Moreover, textual descriptions may specify relationships between parts (e.g. “holding a bag” and “a bag cross chest” in Figure 4(b)). In this case, the correlation between parts is vital for differentiating the two phrases.

Here, we introduce the multi-view non-local network (MV-NLN) to address these problems. In the following,

we take the  $k$ -th visual part feature as an example. As illustrated in Figure 4(c), we first compute the similarity between  $\mathbf{v}_l^k$  and  $\mathbf{v}_l^i (i \neq k)$  in a shared embedding space via multi-view projections:

$$S_{ki} = \frac{\theta_k(\mathbf{v}_l^k)^T \phi_i(\mathbf{v}_l^i)}{\|\theta_k(\mathbf{v}_l^k)\| \|\phi_i(\mathbf{v}_l^i)\|}, \quad (13)$$

where  $\theta_k(\mathbf{v}_l^k) = \mathbf{W}_\theta^k \mathbf{v}_l^k$ ,  $\phi_i(\mathbf{v}_l^i) = \mathbf{W}_\phi^i \mathbf{v}_l^i$ .  $\mathbf{W}_\theta^k, \mathbf{W}_\phi^i \in \mathbb{R}^{M' \times M}$ . Then, the interaction strength between the  $k$ -th visual part feature and the other  $K-1$  part features can thus be denoted as follows:

$$\alpha_{ki} = \frac{\exp(S_{ki})}{\sum_{i=1, i \neq k}^K \exp(S_{ki})}, \quad (14)$$

and  $\alpha_{ki}$  is utilized to aggregate the  $K-1$  part features:

$$\mathbf{v}_{l_{in}}^k = \mathbf{W}_\gamma^k \left( \sum_{i=1, i \neq k}^K \alpha_{ki} \phi_i(\mathbf{v}_l^i) \right). \quad (15)$$

Finally, the part-level visual features produced by MV-NLN can be denoted as follows:

$$\mathbf{v}_n^k = \mathbf{W}_n^k (\mathbf{v}_l^k + \mathbf{v}_{l_{in}}^k), \quad (16)$$

where  $\mathbf{W}_n^k \in \mathbb{R}^{N \times M}$  and  $\mathbf{W}_\gamma^k \in \mathbb{R}^{M \times M'}$ .

Similar to the visual features, we also process the part-level textual features by using MV-NLN to capture their correlations. Note that the parameters of MV-NLN are shared between the two modalities. Similar to  $S_g$  and  $S_l$ , we adopt the cosine metric to evaluate the similarity between the features produced by MV-NLN for one image-text pair:

$$S_n = \frac{\mathbf{v}_n^T \mathbf{t}_n}{\|\mathbf{v}_n\| \|\mathbf{t}_n\|}, \quad (17)$$

where  $\mathbf{v}_n$  and  $\mathbf{t}_n$  are obtained by concatenating the  $K$  part-level visual and textual features produced by MV-NLN.

## 4. Optimization

The popular ranking loss [4] applies a constraint such that the intra-class similarity score must be larger than the inter-class similarity by a margin of  $\alpha$  as follows:

$$L_r = \max(\alpha - S(\mathbf{I}_p, \mathbf{D}_p) + S(\mathbf{I}_p, \mathbf{D}_n), 0) + \max(\alpha - S(\mathbf{I}_p, \mathbf{D}_p) + S(\mathbf{I}_n, \mathbf{D}_p), 0), \quad (18)$$

where  $\mathbf{I}_p$  and  $\mathbf{D}_p$  are drawn from a matching image-text pair.  $\mathbf{D}_n$  and  $\mathbf{I}_n$  denote the hardest negative text for  $\mathbf{I}_p$  and the hardest negative image for  $\mathbf{D}_p$  in a mini-batch, respectively. However, as shown in Figure 1, textual descriptions are flexible. The above ranking loss utilizes only the matching image-text pairs to compose positive pairs, which may result in a risk of overfitting.

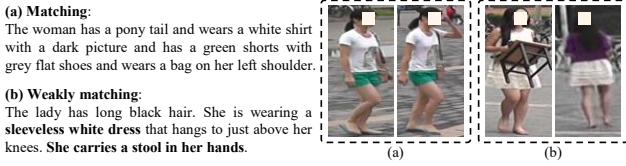


Figure 5. Textual descriptions can roughly annotate the other images of the same identity. However, their descriptive power varies dramatically. (a) The textual description for the left image is also nearly perfect for the right one. (b) The textual description for the left image is only weakly relevant to the right image.

As Figure 5 illustrates, textual descriptions can approximately annotate other images of the same identity; in other words, each textual description can be considered as a coarse caption for the other images of the same identity. Inspired by this observation, we propose a Compound Ranking (CR) loss that includes both strong and weak supervision terms. The positive pairs in strong supervision terms are drawn from image-text pairs that exactly match. By contrast, the positive pairs in weak supervision terms are composed of one image and the textual description for another image of the same identity. In this way, the CR loss exploits more diverse textual descriptions for each training image, which acts as a data augmentation strategy. Formally, the CR loss is defined as follows:

$$\begin{aligned}
 L_{cr} = & \max(\alpha_1 - S(\mathbf{I}_p, \mathbf{D}_p) + S(\mathbf{I}_p, \mathbf{D}_n), 0) \\
 & + \max(\alpha_1 - S(\mathbf{I}_p, \mathbf{D}_p) + S(\mathbf{I}_n, \mathbf{D}_p), 0) \\
 & + \beta \cdot \max(\alpha_2 - S(\mathbf{I}_p, \mathbf{D}'_p) + S(\mathbf{I}_p, \mathbf{D}_n), 0) \\
 & + \beta \cdot \max(\alpha_2 - S(\mathbf{I}_p, \mathbf{D}'_p) + S(\mathbf{I}_n, \mathbf{D}'_p), 0),
 \end{aligned} \quad (19)$$

where  $\mathbf{D}'_p$  refers to the textual description for another image of the same identity as  $\mathbf{I}_p$ .  $\alpha_1$  and  $\alpha_2$  indicate the margins.  $\beta$  denotes the weight for the weak supervision terms.

However, as illustrated in Figure 5, the descriptive power of  $\mathbf{D}'_p$  for  $\mathbf{I}_p$  varies due to the rich intra-class variance in image appearances, indicating that a fixed margin in the two weak supervision terms may be suboptimal. To overcome this problem, we propose the following strategy to adaptively adjust the value of  $\alpha_2$ :

$$\alpha_2 = (\lambda + 1) \frac{\alpha_1}{2}, \quad (20)$$

where

$$\lambda = \min\left(\frac{S(\mathbf{I}_p, \mathbf{D}'_p)}{S(\mathbf{I}_p, \mathbf{D}_p)}, 1\right). \quad (21)$$

The CR loss and the popular ID loss [41] are employed together to optimize the global features, the part features produced by PFL, and the part features produced by PRL, respectively. Note that the ID loss is imposed on each of the  $K$  part features, while the CR loss is imposed on the

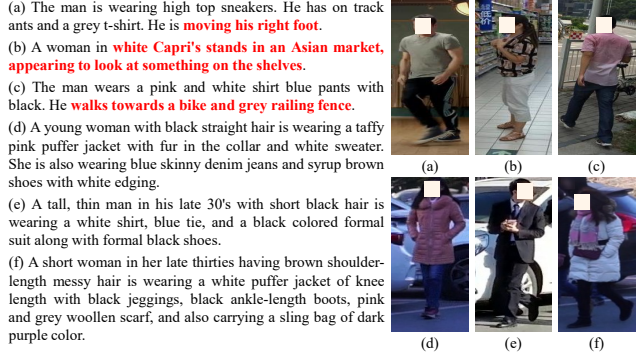


Figure 6. Comparisons between textual descriptions in the CUHK-PEDES and ICFG-PEDES databases. (a)–(c) Descriptions from CUHK-PEDES. The colored words are identity-irrelevant. (d)–(f) Descriptions from ICFG-PEDES show that the descriptions are more fine-grained in this dataset.

concatenated  $K$  part features. The weights of all loss terms for the three types of features are set to 1, 0.5, and 0.5.

In the testing stage, the overall similarity score between one image-text pair is the sum of  $S_g$ ,  $S_l$ , and  $S_n$ .

## 5. Experiments

In this section, we conduct experiments on the CUHK-PEDES database [17], as well as our newly constructed ICFG-PEDES database.

CUHK-PEDES contains 40,206 images and 80,412 textual descriptions for 13,003 identities with two captions per image. There are on average 23.5 words in each textual description. In line with the official evaluation protocol, the training set includes 34,054 images and 68,108 textual descriptions for 11,003 persons. The validation and test sets include data for 1,000 persons, respectively. The images and textual descriptions of the testing data make up the gallery set and probe set, respectively.

As there is only one large-scale database available for text-to-image ReID. It is hard for existing works to reliably verify the effectiveness of text-to-image ReID methods. Moreover, as illustrated in Figure 6, in CUHK-PEDES, textual descriptions may contain identity-irrelevant details (e.g. actions and backgrounds). Therefore, we construct a new database named ICFG-PEDES. The new database contains more identity-centric and fine-grained textual descriptions than CUHK-PEDES. It contains a total of 54,522 pedestrian images of 4,102 identities. All images are gathered from the MSMT17 database [35]. There is one caption per image and there are on average 37.2 words for each description. The database contains a total of 5,554 unique words. Similar to the protocol in the original MSMT17 database, we divide ICFG-PEDES into a training set and a testing set: the former comprises 34,674 image-text pairs of

3,102 persons, while the latter contains 19,848 image-text pairs for the remaining 1,000 persons.

Following [17], we adopt Rank-1, Rank-5, and Rank-10 accuracies to evaluate performance on both databases. In the original protocol of CUHK-PEDES [17], the gallery set includes the exact matching image for each probe textual description; this may reduce the difficulty of text-to-image ReID. In real-world applications, a given textual description may be based on witnesses’ impressions, while the exact matching images are not recorded by cameras. It is therefore valuable to evaluate a model’s ability to search for other images with the same identity except for the exact matching one. Accordingly, we propose a new evaluation metric in which we hide the exact matching image in the gallery for each query description when calculating the Rank-1 accuracy. We name this new metric HMR-1.

### 5.1. Implementation Details

Following a recent text-to-image ReID work [32], we resize all images to  $384 \times 128$  pixels and adopt random horizontal flipping for data augmentation. To facilitate fair comparison with existing approaches, we adopt VGG-16 [27] and ResNet-50 [8] as the visual backbone, respectively; both backbones are pre-trained on the ImageNet database [25]. For textual descriptions, we count the unique words mentioned more than twice to build a vocabulary in the training set. The size of the vocabulary is 4,593 for CUHK-PEDES and 2,474 for ICFG-PEDES. Other important parameters, i.e.  $K$ ,  $V$ ,  $M$ ,  $N$ ,  $M'$ ,  $\alpha_1$ , and  $\beta$ , are empirically set to 6, 512, 1024, 512, 512, 0.2, and 0.1, respectively.

During training, we adopt Adam [12] as the optimizer. We set the batch size and number of epochs to 64 and 60, respectively. The learning rate is initially set as 0.001 and is reduced by multiplying by 0.1 at every 20 epochs.

### 5.2. Comparisons with State-of-the-Art Methods

We compare the performance of SSAN with state-of-the-art methods on the CUHK-PEDES database in Table 1. Most approaches in this table are also part-based [2, 11, 21, 32]. Depending on which visual backbone is adopted, we divide these approaches into two groups: VGG-16-based methods and ResNet-50-based methods. Moreover, the baseline model in this table refers to the model in which we remove all part branches and the CR loss from SSAN; accordingly, the baseline model only extracts global features, as described in Section 3.2. It adopts the cross-entropy loss and ordinary ranking loss for optimization. We can make the following observations from Table 1.

First, thanks to the weight-sharing strategy, our baseline model performs better than that in ViTAA [32]. Without the weight-sharing strategy, our baseline achieves 53.12% Rank-1 accuracy with the ResNet-50 backbone, which is approximately the same as that in ViTAA.

Table 1. Performance Comparisons on CUHK-PEDES

Methods		Rank-1	Rank-5	Rank-10
VGG-16	GNA-RNN [17]	19.05	-	53.64
	IATVM [16]	25.94	-	60.48
	PWM-ATH [2]	27.14	49.45	61.02
	PMA [11]	47.02	68.54	78.06
	MIA [21]	48.00	70.70	79.30
	TDE [22]	52.37	75.26	83.31
<b>SSAN</b>		<b>55.52</b>	<b>76.17</b>	<b>83.45</b>
ResNet-50	Dual Path [41]	44.40	66.26	75.07
	CMPM + CMPC [40]	49.37	-	79.27
	MIA [21]	53.10	75.00	82.90
	PMA [11]	53.81	73.54	81.23
	TDE [22]	55.25	77.46	84.56
	ViTAA [32]	55.97	75.84	83.52
	Baseline in [32]	52.27	73.33	81.61
	Baseline in SSAN	54.68	75.42	82.73
	<b>SSAN</b>		<b>61.37</b>	<b>80.15</b>

Second, SSAN significantly outperforms all existing approaches in terms of Rank-1, Rank-5, and Rank-10 metrics. More specifically, SSAN outperforms the most recent method ViTAA [32] by 5.4% in terms of Rank-1 accuracy. It is worth noting that both ViTAA and SSAN adopt the same input image size and backbones. Of the VGG-16-based methods, SSAN outperforms TDE [22] by 3.15% in terms of Rank-1 accuracy. Another advantage of SSAN is its ability to automatically extract semantically aligned part features from both modalities. By comparison, the other methods typically rely on external tools to extract part-level textual features [11, 21, 32]. These comparisons demonstrate the effectiveness of SSAN.

### 5.3. Ablation Study

We next conduct ablation experiments to explore the effectiveness of each key component of SSAN, i.e. PFL, PRL, and CR loss. The experimental results are shown in Table 2. **Effectiveness of PFL.** In this experiment, we equip the baseline model with  $K$  part branches adopting the PFL module alone. As shown in Table 2, PFL promotes the Rank-1 accuracy of the baseline model by 4.58% and 3.56% on CUHK-PEDES and ICFG-PEDES, respectively; it also promotes the HMR-1 accuracy by 4.24% and 3.46% on the two databases, respectively. Furthermore, when using the same ResNet-50 visual backbone, our PFL approach consistently outperforms state-of-the-art part-based methods [11, 21, 32], as shown in Table 2. The above comparisons demonstrate the effectiveness of PFL for automatically learning semantically aligned part-level features.

**Effectiveness of PRL.** We next equip the baseline with both PFL and MV-NLN. As shown in Table 2, PRL further improves ReID performance by 1.33% and 0.95% in terms of

Table 2. Ablation Study on Each Component of SSAN

Dataset	Components				CUHK-PEDES			ICFG-PEDES		
	Metric	Global	PFL	MV-NLN	CR loss	Rank-1	Rank-5	HMR-1	Rank-1	Rank-5
Baseline	✓	-	-	-	54.68	75.42	42.10	49.02	69.05	44.43
+ PFL	✓	✓	-	-	59.26	78.56	46.34	52.58	71.70	47.89
+ PFL + PRL	✓	✓	✓	-	60.59	79.37	47.21	53.53	72.38	49.04
+ PFL+1×1 Conv	✓	✓	-	-	59.36	79.06	46.51	52.63	72.05	47.97
+ CR loss	✓	-	-	✓	56.30	77.21	44.65	50.23	69.56	46.25
SSAN	✓	✓	✓	✓	<b>61.37</b>	<b>80.15</b>	<b>49.11</b>	<b>54.23</b>	<b>72.63</b>	<b>50.18</b>

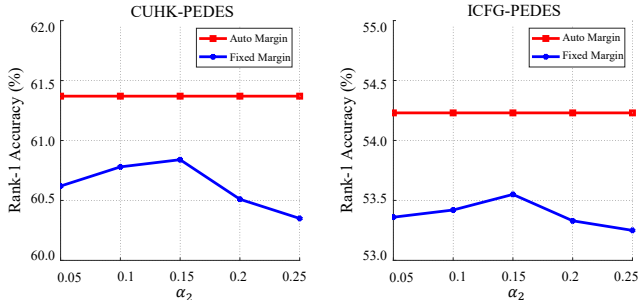


Figure 7. Comparisons between adaptive margins and fixed margins for the weak supervision terms in the CR loss.

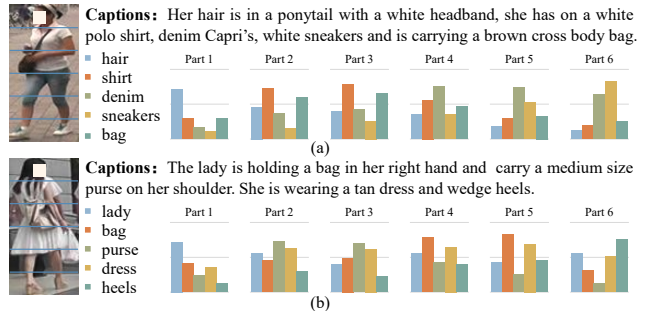
Rank-1 accuracy on CUHK-PEDES and ICFG-PEDES respectively. It also promotes the HMR-1 accuracy by 0.87% and 1.15% on the two databases, respectively.

To ensure that SSAN benefits from the use of correlations between parts, we remove all layers except for the last  $1 \times 1$  Conv of MV-NLN in PRL; the other experimental settings remain the same. As shown in Table 2, this model yields limited performance improvements on both databases, which indicate that the improvements achieved by PRL are due to its part-relation modeling ability.

**Effectiveness of CR loss.** We next explore the effectiveness of the CR loss. As shown in Table 2, the CR loss promotes the Rank-1 accuracy of the baseline model by 1.62% and 1.21% on CUHK-PEDES and ICFG-PEDES, respectively. Moreover, by reducing the intra-class variance of textual features, the CR loss improves the HMR-1 accuracy by 2.55% and 1.82% on the two databases.

Furthermore, we equip the baseline model with PFL, MV-NLN, and the CR loss together, referred to as SSAN in Table 2. Compared with the model that uses PFL and MV-NLN alone, the CR loss promotes the Rank-1 accuracy by 0.78% and 0.7%, while the HMR-1 accuracy is improved by 1.9% and 1.14% on the two benchmarks.

Finally, we provide comparisons between adaptive margins and fixed margins for the weak supervision terms in the CR loss. As illustrated in Figure 7, SSAN with adaptive margins consistently outperforms SSAN with fixed margins on both databases. The above comparisons demonstrate the

Figure 8. Illustration of WAM’s prediction regarding the probability that one word belongs to each of the  $K$  body parts.

effectiveness of the proposed CR loss.

## 5.4. Qualitative Results

We present the prediction scores obtained by WAM for some representative words in Figure 8. Each score denotes the probability that one word belongs to a certain body part. From the figure, we can make the following observations.

First, supervised by well-aligned parts in images, WAM makes correct predictions for words that correspond to fixed body parts. For example, as illustrated in Figure 8(a), the word “shirt” has high scores for the second and third parts.

Second, by utilizing the contextual cues, WAM also makes reasonable predictions for words that correspond to objects with flexible positions. For example, the word “bag” in the phrase “a cross body bag” has high scores on the second and third parts in Figure 8(a). By contrast, the word “bag” in the phrase “a bag in her right hand” has high scores on the fourth and fifth parts in Figure 8(b). The above qualitative results demonstrate the reliability of WAM.

## 6. Conclusion

In this paper, we propose a novel model, named SSAN, to automatically extract semantically aligned features from the visual and textual modalities for text-to-image ReID. Specifically, we introduce a word attention module that reliably attends to part-relevant words. This enables SSAN to automatically extract part-level features for the two modalities by shared  $1 \times 1$  Conv layers. We further propose a



multi-view non-local network to capture the relationships between body parts. Moreover, to overcome the large intra-class variance problem in textual descriptions, we propose a CR loss including both strong and weak supervision terms. Finally, to expedite research in text-to-image ReID, we build a new database that features identity-centric and fine-grained textual descriptions. Extensive experiments on two databases demonstrate the effectiveness of SSAN.

## References

- [1] Hui Chen, Guiguang Ding, Xudong Liu, Zijia Lin, Ji Liu, and Jungong Han. Imram: Iterative matching with recurrent attention memory for cross-modal image-text retrieval. In *Proceedings of the IEEE Conference on Computer Vision and Pattern Recognition*, pages 12655–12663, 2020.
- [2] Tianlang Chen, Chenliang Xu, and Jiebo Luo. Improving text-based person search by spatial matching and adaptive threshold. In *2018 IEEE Winter Conference on Applications of Computer Vision*, pages 1879–1887. IEEE, 2018.
- [3] Changxing Ding, Kan Wang, Pengfei Wang, and Dacheng Tao. Multi-task learning with coarse priors for robust part-aware person re-identification. *T-PAMI*, 2020.
- [4] Fartash Faghri, David J Fleet, Jamie Ryan Kiros, and Sanja Fidler. Vse++: Improving visual-semantic embeddings with hard negatives. 2018.
- [5] Andrea Frome, Greg S Corrado, Jon Shlens, Samy Bengio, Jeff Dean, Marc’Aurelio Ranzato, and Tomas Mikolov. Devise: A deep visual-semantic embedding model. In *Advances in Neural Information Processing Systems*, pages 2121–2129, 2013.
- [6] Jing Ge, Guangyu Gao, and Zhen Liu. Visual-textual association with hardest and semi-hard negative pairs mining for person search. *arXiv preprint arXiv:1912.03083*, 2019.
- [7] Jiuxiang Gu, Jianfei Cai, Shafiq R Joty, Li Niu, and Gang Wang. Look, imagine and match: Improving textual-visual cross-modal retrieval with generative models. In *Proceedings of the IEEE Conference on Computer Vision and Pattern Recognition*, pages 7181–7189, 2018.
- [8] Kaiming He, Xiangyu Zhang, Shaoqing Ren, and Jian Sun. Deep residual learning for image recognition. In *Proceedings of the IEEE Conference on Computer Vision and Pattern Recognition*, pages 770–778, 2016.
- [9] Geoffrey E Hinton, Terrence Joseph Sejnowski, and Tomaso A Poggio. *Unsupervised learning: foundations of neural computation*. MIT press, 1999.
- [10] Yan Huang, Qi Wu, Chunfeng Song, and Liang Wang. Learning semantic concepts and order for image and sentence matching. In *Proceedings of the IEEE Conference on Computer Vision and Pattern Recognition*, pages 6163–6171, 2018.
- [11] Ya Jing, Chenyang Si, Junbo Wang, Wei Wang, Liang Wang, and Tieniu Tan. Pose-guided multi-granularity attention network for text-based person search. In *AAAI*, 2020.
- [12] Diederik P Kingma and Jimmy Ba. Adam: A method for stochastic optimization. *Proceedings of the International Conference on Learning Representations*, 2015.
- [13] Benjamin Klein, Guy Lev, Gil Sadeh, and Lior Wolf. Associating neural word embeddings with deep image representations using fisher vectors. In *Proceedings of the IEEE Conference on Computer Vision and Pattern Recognition*, pages 4437–4446, 2015.
- [14] Kuang-Huei Lee, Xi Chen, Gang Hua, Houdong Hu, and Xiaodong He. Stacked cross attention for image-text matching. In *Proceedings of the European Conference on Computer Vision (ECCV)*, pages 201–216, 2018.
- [15] Qingming Leng, Mang Ye, and Qi Tian. A survey of open-world person re-identification. *IEEE Transactions on Circuits and Systems for Video Technology*, 30(4):1092–1108, 2019.
- [16] Shuang Li, Tong Xiao, Hongsheng Li, Wei Yang, and Xiaogang Wang. Identity-aware textual-visual matching with latent co-attention. In *Proceedings of the IEEE International Conference on Computer Vision*, pages 1890–1899, 2017.
- [17] Shuang Li, Tong Xiao, Hongsheng Li, Bolei Zhou, Dayu Yue, and Xiaogang Wang. Person search with natural language description. In *Proceedings of the IEEE Conference on Computer Vision and Pattern Recognition*, pages 1970–1979, 2017.
- [18] Chunxiao Liu, Zhendong Mao, Tianzhu Zhang, Hongtao Xie, Bin Wang, and Yongdong Zhang. Graph structured network for image-text matching. In *Proceedings of the IEEE Conference on Computer Vision and Pattern Recognition*, pages 10921–10930, 2020.
- [19] Jiawei Liu, Zheng-Jun Zha, Richang Hong, Meng Wang, and Yongdong Zhang. Deep adversarial graph attention convolution network for text-based person search. In *ACM Multimedia Conference on Multimedia Conference*, pages 665–673, 2019.
- [20] Edward Loper and Steven Bird. Nltk: the natural language toolkit. *ACL*, 2004.
- [21] Kai Niu, Yan Huang, Wanli Ouyang, and Liang Wang. Improving description-based person re-identification by multi-granularity image-text alignments. *IEEE Transactions on Image Processing*, 29:5542–5556, 2020.
- [22] Kai Niu, Yan Huang, and Liang Wang. Textual dependency embedding for person search by language. In *Proceedings of the 28th ACM International Conference on Multimedia*, pages 4032–4040, 2020.
- [23] Zhenxing Niu, Mo Zhou, Le Wang, Xinbo Gao, and Gang Hua. Hierarchical multimodal lstm for dense visual-semantic embedding. In *Proceedings of the IEEE International Conference on Computer Vision*, pages 1881–1889, 2017.
- [24] Leigang Qu, Meng Liu, Da Cao, Liqiang Nie, and Qi Tian. Context-aware multi-view summarization network for image-text matching. In *ACM Multimedia Conference on Multimedia Conference*, pages 1047–1055, 2020.
- [25] Olga Russakovsky, Jia Deng, Hao Su, Jonathan Krause, Sanjeev Satheesh, Sean Ma, Zhiheng Huang, Andrej Karpathy, Aditya Khosla, and Michael Bernstein. Imagenet large scale visual recognition challenge. *International Journal of Computer Vision*, 115(3):211–252, 2015.
- [26] Nikolaos Sarafianos, Xiang Xu, and Ioannis A Kakadiaris. Adversarial representation learning for text-to-image match-

- ing. In *Proceedings of the IEEE International Conference on Computer Vision*, pages 5814–5824, 2019.
- [27] Karen Simonyan and Andrew Zisserman. Very deep convolutional networks for large-scale image recognition. *Proceedings of the International Conference on Learning Representations*, 2015.
- [28] Yifan Sun, Liang Zheng, Yi Yang, Qi Tian, and Shengjin Wang. Beyond part models: Person retrieval with refined part pooling (and a strong convolutional baseline). In *Proceedings of the European Conference on Computer Vision*, pages 480–496, 2018.
- [29] Kan Wang, Pengfei Wang, Changxing Ding, and Dacheng Tao. Batch coherence-driven network for part-aware person re-identification. *IEEE Transactions on Image Processing*, 30:3405–3418, 2021.
- [30] Liwei Wang, Yin Li, and Svetlana Lazebnik. Learning deep structure-preserving image-text embeddings. In *Proceedings of the IEEE Conference on Computer Vision and Pattern Recognition*, pages 5005–5013, 2016.
- [31] Xiaolong Wang, Ross Girshick, Abhinav Gupta, and Kaiming He. Non-local neural networks. In *Proceedings of the IEEE Conference on Computer Vision and Pattern Recognition*, pages 7794–7803, 2018.
- [32] Zhe Wang, Zhiyuan Fang, Jun Wang, and Yezhou Yang. Vi-taa: Visual-textual attributes alignment in person search by natural language. 2020.
- [33] Zihao Wang, Xihui Liu, Hongsheng Li, Lu Sheng, Junjie Yan, Xiaogang Wang, and Jing Shao. Camp: Cross-modal adaptive message passing for text-image retrieval. In *Proceedings of the IEEE International Conference on Computer Vision*, pages 5764–5773, 2019.
- [34] Zheng Wang, Zhixiang Wang, Yinqiang Zheng, Yang Wu, Wenjun Zeng, and Shin’ichi Satoh. Beyond intra-modality: A survey of heterogeneous person re-identification. *Proceedings of the International Joint Conferences on Artificial Intelligence*, 2020.
- [35] Longhui Wei, Shiliang Zhang, Wen Gao, and Qi Tian. Person transfer gan to bridge domain gap for person re-identification. In *Proceedings of the IEEE Conference on Computer Vision and Pattern Recognition*, pages 79–88, 2018.
- [36] Xi Wei, Tianzhu Zhang, Yan Li, Yongdong Zhang, and Feng Wu. Multi-modality cross attention network for image and sentence matching. In *Proceedings of the IEEE Conference on Computer Vision and Pattern Recognition*, pages 10941–10950, 2020.
- [37] Fei Yan and Krystian Mikolajczyk. Deep correlation for matching images and text. In *Proceedings of the IEEE Conference on Computer Vision and Pattern Recognition*, pages 3441–3450, 2015.
- [38] Hantao Yao, Shiliang Zhang, Richang Hong, Yongdong Zhang, Changsheng Xu, and Qi Tian. Deep representation learning with part loss for person re-identification. *IEEE Transactions on Image Processing*, 28(6):2860–2871, 2019.
- [39] Qi Zhang, Zhen Lei, Zhaoxiang Zhang, and Stan Z Li. Context-aware attention network for image-text retrieval. In *Proceedings of the IEEE Conference on Computer Vision and Pattern Recognition*, pages 3536–3545, 2020.
- [40] Ying Zhang and Huchuan Lu. Deep cross-modal projection learning for image-text matching. In *Proceedings of the European Conference on Computer Vision*, pages 686–701, 2018.
- [41] Zhedong Zheng, Liang Zheng, Michael Garrett, Yi Yang, Mingliang Xu, and Yi-Dong Shen. Dual-path convolutional image-text embeddings with instance loss. *Proceedings of the ACM Transactions on Multimedia Computing, Communications, and Applications*, 16(2):1–23, 2020.